International Journal of Thermophysics, Vol. 25, No. 3, May 2004 (© 2004)

Relationships Among Liquid–Vapor Interfacial Region Properties: Predictions of a Thermodynamic Model

V. P. Carey[1,2] and A. P. Wemhoff[1]

Received September 9, 2003

In theoretical models and molecular dynamics simulations of the interfacial region between a liquid and vapor phase, three properties are usually of primary interest: the interfacial tension, the interfacial region thickness, and the density gradient in the interfacial region. While these properties can be determined from molecular dynamics simulations by collecting appropriate statistics, such results do not explicitly provide an indication of the interrelationship among these characteristics. This paper presents theoretical predictions of the relationships among interfacial tension, the interfacial region thickness, and the density gradient in the interfacial region that are derived from a theoretical model of the thermodynamic properties of the interfacial region. Explicit relations among interfacial region properties are obtained from a modified version of the classical mean field model that incorporates Redlich-Kwong fluid properties. Comparisons are presented that indicate that the theoretical relations among the interfacial region properties are consistent with trends indicated by experimental data. Use of the theoretical model relations to determine the interfacial tension using the mean density profile obtained from a molecular dynamics simulation is also explored. This method is shown to predict values comparable to traditional methods for determining interfacial tension in molecular dynamics simulations while requiring significantly less computational effort.

KEY WORDS: interfacial region; molecular dynamics; Redlich–Kwong; surface tension; thermodynamic properties.

1. INTRODUCTION

Recent theoretical and experimental investigations of the interfacial region between a liquid and vapor phase have provided detailed information

[1] Department of Mechanical Engineering, University of California, Berkeley, California 94720-1740, U.S.A.
[2] To whom correspondence should be addressed. E-mail: vcarey@me.berkeley.edu

0195-928X/04/0500-0753/0

about the characteristics of the interfacial region. Over the past decade, use of molecular dynamics simulations to explore interfacial region thermophysics has grown in tandem with the increase in accessible computing power to do such calculations. There have been a number of recent molecular dynamics simulation studies of interfacial region properties. These include investigations by Matsumoto et al. [1–4], Dang and Chang [5], Chen et al. [6] and Tarek et al. [7]. Simulations of this type have typically been statistically analyzed to determine the interfacial free energy σ_{lv} and the interfacial region thickness δz_i. There are extensive interfacial tension data reported in the literature (see the discussion in Poling et al. [8]) and recent experimental investigations, such as those by Beysens and Robert [9], have directly measured the interfacial region thickness. Comparisons of simulation predictions with measured interfacial tension data and interfacial region thickness data have contributed to the understanding of the thermophysics of the interfacial region.

Another feature of interest is the density profile in the interfacial region. The characteristics of this profile are often quantified in terms of the density gradient at the $z = 0$ location (center) of the interfacial region (defined in Section 2). Because the density profile is steep and nearly linear over much of the central part of the interfacial region, the gradient $(d\hat{\rho}/dz)_{z=0}$ is a quantitative indicator of the nature of the density profile there.

While the results of molecular dynamics simulation studies can be used to infer the relationships among the three parameters σ_{lv}, δz_i and $(d\hat{\rho}/dz)_{z=0}$, they do not provide an explicit indication of how the parameters are related. In contrast, an approximate theoretical model, such as the van der Waals theory of capillarity, can be used to derive explicit relations among these parameters. The predictions of the van der Waals theory are qualitatively similar to real fluid behavior, but its numerical predictions are known to be inaccurate, both in terms of specific property values and the trends in the variations of properties with temperature. Carey [10] has recently described a classical thermodynamic theoretical model of the interfacial region based on Redlich-Kwong fluid properties. This neoclassical Redlich-Kwong fluid model was shown to predict property variations with temperature that agree better with measured data for real fluids (see Carey [10]). The investigation by Carey [10] compared the model predictions of surface tension and interfacial region thickness to corresponding experimental data.

In the investigation summarized here, a model similar to that evaluated by Carey [10] is used to develop theoretical relationships among the three interfacial region properties of primary interest: interfacial tension, interfacial region thickness and core density gradient. The relations so obtained provide insight into the relations that should be present in exper-

imental data. The relations are compared to available data and a relation linking surface tension and interfacial region thickness developed by Hey and Wood [11]. Use of the relations developed here to determine interfacial tension values from density profile data from molecular dynamics simulations is also explored.

2. THERMODYNAMIC ANALYSIS OF THE INTERFACIAL REGION

The model analysis for thermodynamic properties in the interfacial region developed here is similar to the neoclassical theory of capillarity developed by Carey [10] using the Redlich-Kwong model of fluid properties. As in the van der Waals theory of capillarity, in this model the $z=0$ location in the interfacial region is chosen so that

$$\int_{-\infty}^{0} (\hat{\rho}-\hat{\rho}_v)dz + \int_{0}^{\infty} (\hat{\rho}-\hat{\rho}_l)\,dz = 0 \tag{1}$$

In this analysis, ρ is the local mean number density in the interfacial region. The molar density is then given by $\hat{\rho}=\rho/N_{\mathrm{A}}$, where N_{A} is Avogadro's number. Equation (1) assures that the mass in the interfacial region with a distributed density profile is the same as would exist in the region with a discontinuous density step change at $z=0$. The free energy per unit volume is defined as

$$\psi = F/V \tag{2}$$

Here F is the Helmholtz free energy and V represents the volume of a local system within the interfacial region. The interfacial free energy σ is the free energy (per unit area of interface) above that for a step change in $\hat{\rho}$ and ψ at the interface at $z=0$ (see Fig. 1). It follows that

$$\sigma = \int_{-\infty}^{0} [\psi - \psi(\hat{\rho}_v)]\,dz + \int_{0}^{\infty} [\psi - \psi(\hat{\rho}_l)]\,dz \tag{3}$$

With some manipulation, it can be shown that the two-part integral above can be written in the form,

$$\sigma = \int_{-\infty}^{\infty} \left[\psi(\hat{\rho}(z)) - \psi_{\mathrm{sla}}(\hat{\rho}(z))\right] dz \tag{4}$$

where ψ_{sla} is the straight-line approximation of ψ between $\hat{\rho}_v$ and $\hat{\rho}_l$,

$$\psi_{\mathrm{sla}} = \psi(\hat{\rho}_v) + \left[\frac{\psi(\hat{\rho}_v)-\psi(\hat{\rho}_l)}{\hat{\rho}_v-\hat{\rho}_l}\right](\hat{\rho}-\hat{\rho}_v) \tag{5}$$

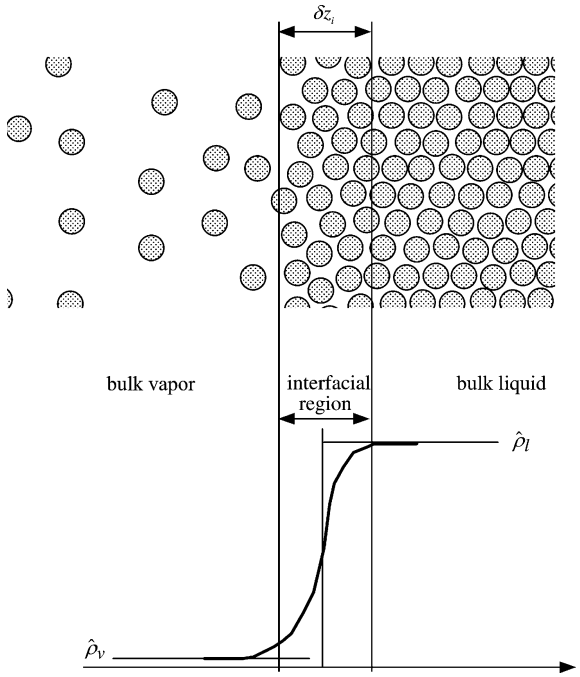

Fig. 1. Variation of the molar density across the interfacial region.

Using the definition of ψ and the fact that for a pure substance the specific Gibbs function is equal to the chemical potential, the following equivalent form of Eq. (5) can be derived:

$$\psi_{\text{sla}} = \hat{\mu}_v \hat{\rho} - P_{\text{sat}} \tag{6}$$

In Eq. (6), P_{sat} is the equilibrium saturation pressure and $\hat{\mu}_v$ is the molar chemical potential for the saturated bulk vapor. Equation (4) implies that the interfacial free energy is associated with the difference between the actual variation of ψ and the straight-line approximation. The interfacial tension or interfacial free energy σ_{lv} is the value of the integral on the right side of Eq. (4) for $\hat{\rho}(z)$ that satisfies Eq. (1) and minimizes the integral. Note that the model analysis used here is similar to the classic van der Waals model of capillarity in that the temperature is taken to be constant in the interfacial region, and the model invokes the global requirement that equilibrium corresponds to the density variation that minimizes the excess free energy.

To evaluate ψ and other properties, a model of the fluid thermophysics is needed. Using Rayleigh's model to account for the density gradient

and the Redlich-Kwong model for fluid properties (see Appendix A), the following relation is obtained for the partition function in the interfacial region:

$$\ln Q = N + \left(\frac{3N}{2}\right)\ln\left[\frac{2\pi M k_{\mathrm{B}} T\,(V - Nb_R)^{2/3}}{N^{2/3}h^2}\right] + N\left[\frac{\xi - 5}{2}\ln\pi - \ln\sigma_s\right] + \frac{(\xi - 3)N}{2}\ln\left(\frac{T}{\theta_{\mathrm{rot,m}}}\right) + \frac{a_{R0}N}{b_R k_{\mathrm{B}} T^{3/2}}\ln\left(\frac{V + Nb_R}{V}\right) + \frac{a_{R0}\kappa V\rho''(z)}{2b_R k_B T^{3/2}}\ln\left(\frac{V + Nb_R}{V}\right) \tag{7}$$

In the above equation, h is Planck's constant, M is the molecular mass of the molecule, N is the number of molecules in a volume V, ξ is the number of translational and rotational storage modes, σ_s is the symmetry number for the molecule,$\theta_{\mathrm{rot},m}$ is the mean rotational temperature for the molecule if it is a polyatomic species, a_{R0} and b_R are the constants in the Redlich-Kwong equation of state for a fluid of uniform density and

$$\kappa = \frac{a_{R1}\gamma_1\eta_1}{a_{R0}\gamma_0\eta_0} = \frac{-\frac{2\pi}{3}\int_{r_{\min}}^{r_{\max}}\phi(r)r^4\,dr}{-2\pi\int_{r_{\min}}^{r_{\max}}\phi(r)r^2\,dr} \tag{8}$$

Consistent with the usual idealizations of mean field theory models, local thermodynamic equilibrium is assumed at each location in the interfacial region. Thermodynamic properties obtained using Eq. (7) are assumed to be valid at each point in the region based on the idealization of local thermodynamic equilibrium. As discussed in Appendix A, the Redlich-Kwong model implicitly embodies the assumption that the integral in the denominator of the right side of Eq. (8) is a function of temperature and density. Note that in the classical van der Waals model, each of these two integrals, and hence their ratio, is constant. At this point, we will take κ to be an unknown function of temperature and density. Later we will show that it is possible to model its dependence on these parameters.

Equation (7) for the partition function applies to a system in which the density varies with z location, as is the case in the interfacial region. Using this result in the thermodynamic relation,

$$F = -k_{\mathrm{B}} T \ln Q \tag{9}$$

together with Eq. (2), and using the definition of the molar density,

$$\hat{\rho} = \rho/N_{\mathrm{A}} = (N/N_{\mathrm{A}})/V \tag{10}$$

the following relation is obtained for ψ:

$$\psi = -\hat{\rho}RT\left[1+\frac{\xi-5}{2}\ln\pi-\ln\sigma_s\right]-\hat{\rho}RT\ln\left[\frac{1-\hat{\rho}N_{\mathrm{A}}b_R}{\hat{\rho}N_{\mathrm{A}}\Lambda^3}\right] -\left(\frac{\xi-3}{2}\right)\hat{\rho}RT\ln\left(\frac{T}{\theta_{\mathrm{rot,m}}}\right) -\frac{a_{R0}N_{\mathrm{A}}^2\hat{\rho}}{N_{\mathrm{A}}b_RT^{1/2}}\ln\left(1+\hat{\rho}N_Ab_R\right)-\frac{a_{R0}N_{\mathrm{A}}^2\kappa\hat{\rho}''(z)}{2N_{\mathrm{A}}b_RT^{1/2}}\ln\left(1+\hat{\rho}N_Ab_R\right) \quad (11)$$

In Eq. (11), Λ is defined as

$$\Lambda=\left[\frac{h^2}{2\pi Mk_{\mathrm{B}}T}\right]^{1/2} \quad (12)$$

Note that in deriving Eq. (11), the molecular number density gradient has been converted to a molar density gradient, making use of the relation,

$$\rho''=\frac{d^2\rho}{dz^2}=N_A\frac{d^2\hat{\rho}}{dz^2}=N_A\hat{\rho}'' \quad (13)$$

In a similar fashion, the thermodynamic relation for the molecular chemical potential μ,

$$\mu=-k_{\mathrm{B}}T\left(\frac{\partial(\ln Q)}{\partial N}\right)_{V,T} \quad (14)$$

can be combined with Eq. (7) with ρ'' set to zero to obtain the following relation for the chemical potential μ for a system with zero density gradient:

$$\mu = -k_BT\left[\frac{\xi-5}{2}\ln\pi-\ln\sigma_s\right]-k_{\mathrm{B}}T\ln\left[\frac{V-Nb_R}{N\Lambda^3}\right]+\frac{Nb_Rk_BT}{V-Nb_R} -\frac{(\xi-3)k_{\mathrm{B}}T}{2}\ln\left(\frac{T}{\theta_{\mathrm{rot,m}}}\right)-\frac{a_{R0}}{b_RT^{1/2}}\ln\left(\frac{V+Nb_R}{V}\right) -\frac{a_{R0}}{b_RT^{1/2}}\left(\frac{Nb_R}{V+Nb_R}\right) \quad (15)$$

Using the relation of Eq. (10) for molar density and the following relation for molar chemical potential $\hat{\mu}$,

$$\hat{\mu}=N_{\mathrm{A}}\mu, \quad (16)$$

Eq. (15) for $\hat{\mu}$ can be converted to the form,

$$\hat{\mu} = -RT\left[\frac{\xi-5}{2}\ln\pi-\ln\sigma_s\right]-RT\ln\left[\frac{1-\hat{\rho}N_{\mathrm{A}}b_R}{\hat{\rho}N_A\Lambda^3}\right]+\frac{\hat{\rho}N_{\mathrm{A}}b_RRT}{1-\hat{\rho}N_{\mathrm{A}}b_R}$$

$$-\frac{(\xi-3)RT}{2}\ln\left(\frac{T}{\theta_{\mathrm{rot},m}}\right)$$
$$-\frac{a_{R0}N_A^2}{N_A b_R T^{1/2}}\ln\left(1+\hat{\rho}N_{\mathrm{A}}b_R\right)-\frac{a_{R0}N_A^2}{T^{1/2}}\left(\frac{\hat{\rho}}{1+\hat{\rho}N_{\mathrm{A}}b_R}\right) \tag{17}$$

On the right side of Eq. (11), the last term alone accounts for the effects of nonuniform density. We can therefore consider the volumetric free energy to consist of two parts:

$$\psi=\psi_0(\hat{\rho},T)-m(\hat{\rho},T)\hat{\rho}\hat{\rho}'' \tag{18}$$

where ψ_0 is the value of ψ at local conditions for uniform density

$$\psi_0(\hat{\rho},T)=-\hat{\rho}RT\left[1+\frac{\xi-5}{2}\ln\pi-\ln\sigma_s\right]-\hat{\rho}RT\ln\left[\frac{1-\hat{\rho}N_{\mathrm{A}}b_R}{\hat{\rho}N_{\mathrm{A}}\Lambda^3}\right]$$
$$-\left(\frac{\xi-3}{2}\right)\hat{\rho}RT\ln\left(\frac{T}{\theta_{\mathrm{rot},m}}\right)-\frac{a_{R0}N_{\mathrm{A}}^2\hat{\rho}}{N_{\mathrm{A}}b_R T^{1/2}}\ln\left(1+\hat{\rho}N_{\mathrm{A}}b_R\right) \tag{19}$$

and $m(\hat{\rho},T)\hat{\rho}\hat{\rho}''$ provides the correction for nonuniform density, $m(\hat{\rho},T)$ being defined as

$$m(\hat{\rho},T)=\frac{a_{R0}N_{\mathrm{A}}^2\kappa}{2N_{\mathrm{A}}b_R T^{1/2}\hat{\rho}}\ln\left(1+\hat{\rho}N_{\mathrm{A}}b_R\right) \tag{20}$$

Substituting the right side of Eq. (18) for ψ in Eq. (4), the interfacial free energy relation can be written as

$$\sigma=\int_{-\infty}^{\infty}\left[\psi_0(\hat{\rho},T)-\psi_{\mathrm{sla}}(\hat{\rho},T)-m(\hat{\rho},T)\hat{\rho}\hat{\rho}''\right]dz \tag{21}$$

For a pure fluid, the following differential relation from classical thermodynamics

$$dF=-S\,dT-P\,dV+\mu\,dN \tag{22}$$

and the definition of ψ imply that for constant V and T,

$$d\psi=d\left(\frac{F}{V}\right)=\mu N_{\mathrm{A}}d\left(\frac{N/N_{\mathrm{A}}}{V}\right)=\hat{\mu}\,d\hat{\rho} \tag{23}$$

It follows from basic calculus that

$$\left(\frac{d\psi}{d\hat{\rho}}\right)_{V,T}=\hat{\mu} \tag{24}$$

Integrating the above relation from the vapor density to an arbitrary density in the interfacial region where the chemical potential is constant yields

$$\psi_{\mathrm{sla}}(\hat{\rho}, T) = \psi_0(\hat{\rho}_v, T) + \hat{\mu}_v(\hat{\rho} - \hat{\rho}_v) \tag{25}$$

Substituting the right side of the above equation for ψ_{sla} in Eq. (21), the resulting equation for the interfacial free energy can be written in the form

$$\sigma = \int_{-\infty}^{\infty} \left[\psi_{\mathrm{e}} - m\hat{\rho}\hat{\rho}''\right] dz \tag{26}$$

where ψ_{e} is the excess volumetric free energy defined as

$$\psi_{\mathrm{e}} = \psi_0(\hat{\rho}, T) - \psi_0(\hat{\rho}_v, T) - \hat{\mu}_v(\hat{\rho} - \hat{\rho}_v) \tag{27}$$

and $\hat{\mu}_v$ is determined from Eq. (17) as

$$\begin{aligned}\hat{\mu}_v = {} & -RT\left[\frac{\xi - 5}{2}\ln\pi - \ln\sigma_s\right] - RT\ln\left[\frac{1 - \hat{\rho}_v N_{\mathrm{A}} b_R}{\hat{\rho}_v N_{\mathrm{A}} \Lambda^3}\right] \\ & + \frac{\hat{\rho}_v N_{\mathrm{A}} b_R RT}{1 - \hat{\rho}_v N_{\mathrm{A}} b_R} - \frac{(\xi - 3)RT}{2}\ln\left(\frac{T}{\theta_{\mathrm{rot,m}}}\right) \\ & - \frac{a_{R0} N_{\mathrm{A}}^2}{N_{\mathrm{A}} b_R T^{1/2}}\ln\left(1 + \hat{\rho}_v N_{\mathrm{A}} b_R\right) - \frac{a_{R0} N_{\mathrm{A}}^2}{T^{1/2}}\left(\frac{\hat{\rho}_v}{1 + \hat{\rho}_v N_{\mathrm{A}} b_R}\right)\end{aligned} \tag{28}$$

With some straightforward manipulation of the density derivatives in the integrand, it can easily be shown that Eq. (26) can be reorganized to the form,

$$\sigma = \int_{-\infty}^{\infty} \left[\psi_{\mathrm{e}} + \frac{1}{2}\tilde{m}(\hat{\rho}')^2\right] dz \tag{29}$$

where

$$\tilde{m} = 2\left(m + \hat{\rho}\frac{dm}{d\hat{\rho}}\right) = \frac{a_{R0} N_{\mathrm{A}}^2 \kappa}{(1 + \hat{\rho} b_R N_{\mathrm{A}}) T^{1/2}} \tag{30}$$

The right side of Eq. (29) equals the equilibrium interfacial free energy when $\hat{\rho}(z)$ is chosen so as to minimize the integral. Application of the calculus of variations to this problem [12] leads to the conclusion that the density profile that minimizes the integral satisfies

$$\hat{\rho}' = \frac{d\hat{\rho}}{dz} = \left(\frac{2\psi_{\mathrm{e}}}{\tilde{m}}\right)^{1/2} \tag{31}$$

and that the minimized integral can be computed as

$$\sigma_{lv} = \int_{-\infty}^{\infty} 2\psi_e(\hat{\rho}, T)\, dz \tag{32}$$

Equation (31) also implies that

$$dz = \left(\frac{2\psi_e}{\tilde{m}}\right)^{-1/2} d\hat{\rho} \tag{33}$$

Substituting the right side of Eq. (33) for dz in Eq. (32), changing the integration variable from z to $\hat{\rho}$, and changing the integration limits accordingly, Eq. (32) becomes

$$\sigma_{lv} = \int_{\hat{\rho}_v}^{\hat{\rho}_l} \left[2\tilde{m}\psi_e(\hat{\rho}, T)\right]^{1/2} d\hat{\rho} \tag{34}$$

It follows from Eq. (34) and the definition of $\tilde{m}$ that

$$\sigma_{lv} = \int_{\hat{\rho}_v}^{\hat{\rho}_l} \left[\frac{2a_{R0}N_A^2\kappa\psi_e(\hat{\rho}, T)}{(1+\hat{\rho}b_R N_A)T^{1/2}}\right]^{1/2} d\hat{\rho} \tag{35}$$

Using Eqs. (19), (27), and (28) to evaluate ψ_e, Eq. (35) can be integrated numerically to predict the interfacial tension, and Eq. (32) can be integrated to predict the variation of density across the interfacial region. To execute such calculations, the fluid constants must be specified and κ defined in Eq. (8) must be determined from a suitable potential function model. The use of this type of model analysis with Redlich-Kwong properties to predict the interfacial tension and property variations across the interface has been explored by Carey [10]. Here, we will instead explore the relationships among interfacial region properties for this type of model in a more explicit way.

Equation (31) can be rearranged to the form,

$$\psi_e = \frac{\tilde{m}}{2}\left(\frac{d\hat{\rho}}{dz}\right)^2 \tag{36}$$

Substituting the right side of Eq. (36) for ψ_e in Eq. (35) yields

$$\sigma_{lv} = \int_{\hat{\rho}_v}^{\hat{\rho}_l} \left[\frac{a_{R0}N_A^2\kappa}{(1+\hat{\rho}b_R N_A)T^{1/2}}\left(\frac{d\hat{\rho}}{dz}\right)\right] d\hat{\rho} \tag{37}$$

Generally, the density profile across the interfacial region predicted by this type of model is characterized by a nearly constant slope in the center of

the region, with the slope rapidly approaching zero at the outer edges of the region. As a first approximation, one could take the gradient to be constant in the integral of Eq. (37) as the density varies from $\hat{\rho}_v$ to $\hat{\rho}_l$. However, the assumption of a constant density gradient through the interfacial region overestimates the value of surface tension. The reason for this inaccuracy lies in the fact that the density gradient is maximum at $z=0$ and decreases to zero in the bulk phases. A simple way to correct this is to assume that the density gradient may be approximated by a quadratic function through the interfacial region:

$$\frac{d\hat{\rho}}{dz} = \left(\frac{d\hat{\rho}}{dz}\right)_{\hat{\rho}=\hat{\rho}_m} \left[1 - 4\left(\frac{\hat{\rho}-\hat{\rho}_m}{\hat{\rho}_l-\hat{\rho}_v}\right)^2\right] \tag{38}$$

where

$$\hat{\rho}_m = (\hat{\rho}_v + \hat{\rho}_l)/2 \tag{39}$$

Note that this approximation is equivalent to assuming that the density profile through the interfacial region is given by

$$\frac{\hat{\rho}-\hat{\rho}_v}{\hat{\rho}_l-\hat{\rho}_v} = \frac{1}{e^{4z/\delta z_i}+1} \tag{40}$$

Placing the density gradient relation Eq. (38) into the integral given by Eq. (37), and performing some calculus, the resulting surface tension relation can be expressed as

$$\sigma_{lv} = \frac{a_{R0}N_A^2\kappa}{b_R N_A}\left(\frac{d\hat{\rho}}{dz}\right)_{\hat{\rho}=\hat{\rho}_m}\left[\ln\frac{1+\hat{\rho}_l b_R N_A}{1+\hat{\rho}_v b_R N_A}\right](1+\eta) \tag{41}$$

where

$$\eta = \frac{15.388 + 2\left(\rho_{r,l}+\rho_{r,v}\right)}{\left(\rho_{r,l}-\rho_{r,v}\right)\ln\left[\frac{3.847+\rho_{r,l}}{3.847+\rho_{r,v}}\right]} - \left[\frac{7.694+\left(\rho_{r,l}+\rho_{r,v}\right)}{\rho_{r,l}-\rho_{r,v}}\right]^2 \tag{42}$$

Note that Eq. (42) is expressed in terms of reduced density. Designating critical properties with a 'c' subscript, we define reduced properties in the usual manner:

$$P_r = P/P_c \tag{43a}$$

$$T_r = T/T_c \tag{43b}$$

$$\rho_r = \hat{\rho}/\hat{\rho}_c \tag{43c}$$

$$v_r = \hat{v}/\hat{v}_c \tag{43d}$$

Table I. Nonlinear Correction to the Constant Density Gradient Approximation

T_r(K)	$\rho_{l,r}$	$\rho_{v,r}$	η	$1+\eta$
0.60	3.025	0.01172	−0.341	0.659
0.70	2.758	0.04559	−0.339	0.661
0.80	2.428	0.1256	−0.338	0.662
0.90	1.987	0.2980	−0.336	0.664
0.95	1.681	0.4643	−0.335	0.665
0.98	1.418	0.6406	−0.334	0.666

Equation (42) allows calculation of η for reduced saturation properties determined using the Redlich-Kwong model of Carey [10] for a wide range of reduced temperatures, and the data are shown in Table I. The data show that $(1+\eta)$ is nearly independent of temperature, and it may be well approximated by the value of 0.66. Therefore, replacing $(1+\eta)$ with 0.66 in Eq. (41) yields a simple but accurate equation relating surface tension to the density gradient at the mean density in the interface:

$$\sigma_{lv} = 0.66 \left(\frac{d\hat{\rho}}{dz}\right)_{\hat{\rho}=\hat{\rho}_m} \frac{a_{R0} N_A^2 \kappa}{b_R N_A T^{1/2}} \ln\left(\frac{1+\hat{\rho}_l b_R N_A}{1+\hat{\rho}_v b_R N_A}\right) \tag{44}$$

Using the definition of ψ_e in Eq. (27) and the property relations above, the following relation for ψ_e is obtained:

$$\begin{aligned}\psi_e = {} & P_{sat} - \hat{\rho} RT \ln\left[\frac{\hat{\rho}_v(1-\hat{\rho} N_A b_R)}{\hat{\rho}(1-\hat{\rho}_v N_A b_R)}\right] \\ & - \frac{a_{R0} N_A^2 \hat{\rho}}{N_A b_R T^{1/2}} \ln\left(\frac{1+\hat{\rho} N_A b_R}{1+\hat{\rho}_v N_A b_R}\right) \\ & - \frac{\hat{\rho} RT}{1-\hat{\rho}_v N_A b_R} + \frac{a_{R0} N_A^2 \hat{\rho}\hat{\rho}_v}{T^{1/2}\left(1+\hat{\rho}_v N_A b_R\right)}\end{aligned} \tag{45}$$

Combining this relation with Eqs. (30) and (31) yields the following relation for the local density gradient in the interfacial region:

$$\begin{aligned}\frac{d\hat{\rho}}{dz} = {} & \left(\frac{2\left(1+\hat{\rho} N_A b_R\right) T^{1/2}}{a_{R0} N_A^2 \kappa}\right)^{1/2} \left[P_{sat} - \hat{\rho} RT \ln\left[\frac{\hat{\rho}_v(1-\hat{\rho} N_A b_R)}{\hat{\rho}(1-\hat{\rho}_v N_A b_R)}\right]\right. \\ & \left. - \frac{a_{R0} N_A^2 \hat{\rho}}{N_A b_R T^{1/2}} \ln\left(\frac{1+\hat{\rho} N_A b_R}{1+\hat{\rho}_v N_A b_R}\right) - \frac{\hat{\rho} RT}{1-\hat{\rho}_v N_A b_R} + \frac{a_{R0} N_A^2 \hat{\rho}\hat{\rho}_v}{T^{1/2}\left(1+\hat{\rho}_v N_A b_R\right)}\right]^{1/2}\end{aligned} \tag{46}$$

The density gradient at the mean density in the layer is obtained by substituting $\hat{\rho}_m$ for $\hat{\rho}$ in Eq. (46),

$$\left(\frac{d\hat{\rho}}{dz}\right)_{\hat{\rho}=\hat{\rho}_m} = \left(\frac{2\left(1+\hat{\rho}_m N_A b_R\right)T^{1/2}}{a_{R0}N_A^2\kappa}\right)^{1/2} \times \left[P_{sat} - \hat{\rho}_m RT \ln\left[\frac{\hat{\rho}_v(1-\hat{\rho}_m N_A b_R)}{\hat{\rho}_m(1-\hat{\rho}_v N_A b_R)}\right] - \frac{a_{R0}N_A^2\hat{\rho}_m}{N_A b_R T^{1/2}}\ln\left(\frac{1+\hat{\rho}_m N_A b_R}{1+\hat{\rho}_v N_A b_R}\right) - \frac{\hat{\rho}_m RT}{1-\hat{\rho}_v N_A b_R} + \frac{a_{R0}N_A^2\hat{\rho}_m\hat{\rho}_v}{T^{1/2}\left(1+\hat{\rho}_v N_A b_R\right)}\right]^{1/2} \tag{47}$$

Substituting the right side of Eq. (47) for the mean density gradient in Eq. (44) yields the following relation for the interfacial tension,

$$\sigma_{lv} = 0.66\frac{a_{R0}N_A^2\kappa}{b_R N_A T^{1/2}}\left(\frac{2\left(1+\hat{\rho}_m N_A b_R\right)T^{1/2}}{a_{R0}N_A^2\kappa}\right)^{1/2}\ln\left(\frac{1+\hat{\rho}_l b_R N_A}{1+\hat{\rho}_v b_R N_A}\right) \times \left[P_{sat} - \hat{\rho}_m RT\ln\left[\frac{\hat{\rho}_v(1-\hat{\rho}_m N_A b_R)}{\hat{\rho}_m(1-\hat{\rho}_v N_A b_R)}\right] - \frac{a_{R0}N_A^2\hat{\rho}_m}{N_A b_R T^{1/2}} \times \ln\left(\frac{1+\hat{\rho}_m N_A b_R}{1+\hat{\rho}_v N_A b_R}\right) - \frac{\hat{\rho}_m RT}{1-\hat{\rho}_v N_A b_R} + \frac{a_{R0}N_A^2\hat{\rho}_m\hat{\rho}_v}{T^{1/2}\left(1+\hat{\rho}_v N_A b_R\right)}\right]^{1/2} \tag{48}$$

It is common to determine the thickness of the interfacial region δz_i as

$$\delta z_i = \frac{(\hat{\rho}_l - \hat{\rho}_v)}{(d\hat{\rho}/dz)_{z=0}} \tag{49}$$

where the derivative is evaluated at the $z=0$ location dictated by Eq. (1). Taking the gradient at $z=0$ to be equal to that at the mean density, a relation for the interfacial region thickness is also obtained by replacing $(d\hat{\rho}/dz)_{z=0}$ in Eq. (49) by the right side of Eq. (47) to obtain

$$\delta z_i = (\hat{\rho}_l - \hat{\rho}_v)\left(\frac{a_{R0}N_A^2\kappa}{2\left(1+\hat{\rho}_m N_A b_R\right)T^{1/2}}\right)^{1/2}\left[P_{\text{sat}} - \hat{\rho}_m RT\ln\left[\frac{\hat{\rho}_v(1-\hat{\rho}_m N_A b_R)}{\hat{\rho}_m(1-\hat{\rho}_v N_A b_R)}\right] - \frac{a_{R0}N_A^2\hat{\rho}_m}{N_A b_R T^{1/2}}\ln\left(\frac{1+\hat{\rho}_m N_A b_R}{1+\hat{\rho}_v N_A b_R}\right) - \frac{\hat{\rho}_m RT}{1-\hat{\rho}_v N_A b_R} + \frac{a_{R0}N_A^2\hat{\rho}_m\hat{\rho}_v}{T^{1/2}\left(1+\hat{\rho}_v N_A b_R\right)}\right]^{-1/2} \tag{50}$$

Using the above relations to replace physical properties (P, T, etc.) with reduced ones (P_r, T_r, etc.), Eqs. (44), (47), (48) and (50) can be converted to the forms,

$$\frac{\sigma_{lv}}{P_c L_i} = 0.66 \frac{a_r}{b_r T_r^{1/2}} \left(\frac{\kappa}{L_i^2}\right) \left(\frac{d\rho_r}{d\zeta}\right)_{\rho_r=\rho_{r,m}} \ln\left(\frac{1+\rho_{r,l} b_r}{1+\rho_{r,v} b_r}\right) \tag{51}$$

$$\left(\frac{d\rho_r}{d\zeta}\right)_{\rho_r=\rho_{r,m}} = \left(\frac{2L_i^2 \left(1+\rho_{r,m} b_r\right) T_r^{1/2}}{a_r \kappa}\right)^{1/2} \left[P_{r,\mathrm{sat}} - \frac{\rho_{r,m}}{3} \ln\left[\frac{\rho_{r,v}(1-\rho_{r,m} b_r)}{\rho_{r,m}(1-\rho_{r,v} b_r)}\right] - \frac{a_r \rho_{r,m}}{b_r T_r^{1/2}} \ln\left(\frac{1+\rho_{r,m} b_r}{1+\rho_{r,v} b_r}\right) - \frac{3\rho_{r,m} T_r}{1-\rho_{r,v} b_r} + \frac{a_r \rho_{r,m} \rho_{r,v}}{T_r^{1/2}\left(1+\rho_{r,v} b_r\right)}\right]^{1/2} \tag{52}$$

$$\frac{\sigma_{lv}}{P_c L_i} = 0.66 \left(\frac{2a_r \kappa \left(1+\rho_{r,m} b_r\right)}{b_r L_i^2 T_r^{1/2}}\right)^{1/2} \ln\left(\frac{1+\rho_{r,l} b_r}{1+\rho_{r,v} b_r}\right) \times \left[P_{r,\mathrm{sat}} - \frac{\rho_{r,m}}{3} \ln\left(\frac{\rho_{r,v}(1-\rho_{r,m} b_r)}{\rho_{r,m}(1-\rho_{r,v} b_r)}\right) - \frac{a_r \rho_{r,m}}{b_r T_r^{1/2}} \ln\left(\frac{1+\rho_{r,m} b_r}{1+\rho_{r,v} b_r}\right) - \frac{3\rho_{r,m} T_r}{1-\rho_{r,v} b_r} + \frac{a_r \rho_{r,m} \rho_{r,v}}{T_r^{1/2}\left(1+\rho_{r,v} b_r\right)}\right]^{1/2} \tag{53}$$

$$\frac{\delta z_i}{L_i} = \left(\rho_{r,l} - \rho_{r,v}\right) \left(\frac{a_r \kappa}{2L_i^2 \left(1+\rho_{r,m} b_r\right) T_r^{1/2}}\right)^{1/2} \times \left[P_{r,sat} - \frac{\rho_{r,m}}{3} \ln\left[\frac{\rho_{r,v}(1-\rho_{r,m} b_r)}{\rho_{r,m}(1-\rho_{r,v} b_r)}\right] - \frac{a_r \rho_{r,m}}{b_r T_r^{1/2}} \ln\left(\frac{1+\rho_{r,m} b_r}{1+\rho_{r,v} b_r}\right) - \frac{3\rho_{r,m} T_r}{1-\rho_{r,v} b_r} + \frac{a_r \rho_{r,m} \rho_{r,v}}{T_r^{1/2}\left(1+\rho_{r,v} b_r\right)}\right]^{-1/2} \tag{54}$$

where

$$L_i = \left(\frac{k_B T_c}{P_c}\right)^{1/3} \tag{55}$$

$$\zeta = z/L_i \tag{56}$$

$$b_r = b_R N_A / \hat{v}_c \tag{57a}$$

$$a_r = a_{R0} N_A^2 / (P_c T_c^{1/2} \hat{v}_c^2) \tag{57b}$$

As indicated in Table II, values of the characteristic length scale L_I are close to 1 nm for a variety of common fluids.

Table II. Values of L_i for Various Fluids

	T_c(K)	P_c(MPa)	L_i(nm)
N_2	126.2	3.400	0.800
CH_4	190.6	4.599	0.830
Ar	150.7	4.865	0.753
O_2	154.5	5.043	0.751
H_2O	647.3	22.129	0.739
NH_3	405.6	11.290	0.793
C_3H_8 (propane)	369.9	4.248	1.063
SF_6	318.7	3.760	1.054
R-134a	374.3	4.059	1.084

As discussed in Appendix A, the partition function used here generates the Redlich–Kwong equation of state

$$P = \frac{Nk_B T}{V - b_R N} - \frac{a_{R0} N^2}{T^{1/2} V (V + b_R N)} \tag{58}$$

which can be reorganized to

$$P = \frac{RT}{\hat{v} - b_R N_A} - \frac{a_{R0} N_A^2}{T^{1/2} \hat{v} (\hat{v} + b_R N_A)} \tag{59}$$

Using this equation of state and invoking the zero slope and inflection point conditions for isotherms on a $P - \hat{v}$ plot passing through the critical point, it can be shown that a_{R0} and b_R are related to the critical temperature and pressure as

$$a_{R0} = 0.42748 \frac{k_B^2 T_c^{2.5}}{P_c} \tag{60a}$$

$$b_R = 0.08664 \frac{k_B T_c}{P_c} \tag{60b}$$

In addition, for a Redlich–Kwong fluid, it is readily shown that

$$\frac{\rho_c k_B T_c}{P_c} = 3 \tag{61}$$

Note that Eqs. (57), (60), and (61) imply that a_r and b_r are just the numerical constants specified below:

$$a_r = 3.84732 \tag{62a}$$

$$b_r = 0.25992 \tag{62b}$$

To computationally evaluate the dimensionless interfacial tension, interfacial region thickness and density gradient for a specified reduced temperature, the reduced saturation pressure and reduced bulk liquid and

vapor densities must first be determined. These properties are determined using the equation of state together with the thermodynamic requirement that the chemical potential in the saturated vapor and liquid must be equal. For specified P_r and T_r, Eq. (59) is a cubic equation for v_r that can be written as

$$v_r^3 - \left(\frac{3T_r}{P_r}\right) v_r^2 + \left(\frac{a_r}{P_r T_r^{1/2}} - b_r^2 - \frac{3b_r T_r}{P_r}\right) v_r - \frac{a_r b_r}{P_r T_r^{1/2}} = 0 \tag{63}$$

Equation (63) can be solved by using numerical methods or by the explicit formulas for roots of a cubic equation. Among the three roots v_{r1}, v_{r2} and v_{r3}, the largest corresponds to the saturated vapor and the smallest corresponds to saturated liquid:

$$v_{r,v} = \max\{v_{r1}, v_{r2}, v_{r3}\} \tag{64a}$$

$$v_{r,l} = \min\{v_{r1}, v_{r2}, v_{r3}\} \tag{64b}$$

Substituting Eqs. (43a)–(43c), the relation of Eq. (17) for the chemical potential can be written in the form,

$$\begin{aligned}\mu_r = &-T_r\left[\frac{\xi-5}{2}\ln\pi - \ln\sigma_s\right] - T_r \ln\left[\frac{1-\rho_r b_r}{\rho_r N_A \Lambda^3 \rho_c}\right] \\ &+ \frac{\rho_r b_r T_r}{1-\rho_r b_r} - \frac{(\xi-3)T_r}{2}\ln\left(\frac{T_r}{T_{\theta,r}}\right) \\ &- \frac{a_r}{3b_r T_r^{1/2}}\ln(1+\rho_r b_r) - \frac{a_r}{3T_r^{1/2}}\left(\frac{\rho_r}{1+\rho_r b_r}\right)\end{aligned} \tag{65}$$

where

$$\mu_r = \frac{\hat{\mu}}{RT_c} \tag{66a}$$

$$T_{\theta,r} = \frac{\theta_{rot,m}}{T_c} \tag{66b}$$

The reduced chemical potential values for saturated vapor and liquid are obtained by evaluating the right side of Eq. (65) for $\rho_{r,v}$ and $\rho_{r,l}$, respectively. For the specified temperature at equilibrium (with no density gradient), $\hat{\mu}_{r,l}$ and $\hat{\mu}_{r,v}$ must be equal. Using Eq. (65) to evaluate the reduced chemical potentials and setting them equal, this requirement can be stated as

$$\begin{aligned}&-T_r \ln\left[\frac{\rho_{r,l}(1-\rho_{r,v}b_r)}{\rho_{r,v}(1-\rho_{r,l}b_r)}\right] + \frac{\rho_{r,v}b_r T_r}{1-\rho_{r,v}b_r} \\ &- \frac{\rho_{r,l}b_r T_r}{1-\rho_{r,l}b_r} - \frac{a_r}{3b_r T_r^{1/2}}\ln\left(\frac{1+\rho_{r,v}b_r}{1+\rho_{r,l}b_r}\right) \\ &- \frac{\rho_{r,v}a_r}{3T_r^{1/2}(1+\rho_{r,v}b_r)} + \frac{\rho_{r,l}a_r}{3T_r^{1/2}(1+\rho_{r,l}b_r)} = 0\end{aligned} \tag{67}$$

Saturation properties can be determined by the iterative method described in Appendix B.

3. DISCUSSION

3.1. Property Relations

Combining the thermodynamic relation linking internal energy and the partition function

$$U = k_B T^2 \left(\frac{\partial (\ln Q)}{\partial T} \right)_{V,N} \tag{68}$$

together with the partition function relation in Eq. (7) with the density gradient set to zero, a relation for the internal energy of the bulk fluid is obtained. Converting the relation to a form for molar specific internal energy and determining the difference between the internal energies of saturated vapor and liquid, the resulting relation is

$$\hat{u}_{lv} = \frac{3 a_{R0} N_A^2}{2 b_R N_A T_r^{1/2}} \ln \left(\frac{1 + \hat{\rho}_l N_A b_R}{1 + \hat{\rho}_v N_A b_R} \right) \tag{69}$$

Solving Eq. (69) for the logarithmic term and substituting to replace the logarithmic term in Eq. (44) yields the following relation for the interfacial tension

$$\sigma_{lv} = 0.44 \kappa \left(\frac{d\hat{\rho}}{dz} \right)_{\hat{\rho}=\hat{\rho}_m} \hat{u}_{lv} \tag{70}$$

Using Eq. (49) to replace the derivative in Eq. (70), we obtain

$$\sigma_{lv} = 0.44 \kappa \left(\frac{\hat{\rho}_l - \hat{\rho}_v}{\delta z_i} \right) \hat{u}_{lv} \tag{71}$$

Equation (71), which links the interfacial tension to the interfacial region thickness, is similar to the relation linking these parameters obtain by Hey and Wood [11] for a van der Waals fluid.

3.2. Prediction of Interfacial Region Thickness

The relations described above that link together the interfacial tension, interfacial region thickness, and the saturation properties are useful in two important ways. One useful application of the above relations is to use them to predict the thickness of the interfacial region from known physical property data. To do so, a means of predicting κ must

be included. Equation (8) can be used to evaluate κ if a model relation for the potential function and the limits of integration are specified. Carey [10] proposed a model for evaluating κ that yields the relation

$$\frac{\kappa}{L_i^2} = 0.1613\,(1 - T/T_c)^{-0.34} \tag{72}$$

(see Appendix C). It should be noted that the value of κ depends on the model potential used. This parameter can be determined from any of a number of possible intermolecular potentials. In this study, the Lennard-Jones 6–12 potential was selected because it is generally acknowledged to be among the more realistic two-parameter potential function models. Because it is a two-parameter model, use of the Lennard-Jones potential is consistent with the two-parameter Redlich-Kwong property model used here. Using Eq. (72) to eliminate κ in Eq. (71) yields

$$\delta z_i = 0.071 L_i^2\,(1 - T/T_c)^{-0.34} \left(\frac{\hat{\rho}_l - \hat{\rho}_v}{\sigma_{lv}}\right) \hat{u}_{lv} \tag{73}$$

Figure 2 shows a plot of the interfacial region thickness predicted using Eq. (73) for a variety of fluids. The data plotted in this figure were computed using saturation properties at several temperatures for each fluid. The saturation property data were taken from recommended values in the ASHRAE Fundamentals Handbook [13]. The computed δz_i values plotted in Fig. 2 indicate that for a variety of common fluids under commonly encountered saturation conditions, the theory described here predicts that the interfacial region thickness is in the range of 1–10 nm. This result, which is consistent with the observed trends in the model of Hey and Wood [11], is remarkable, given that it seems to apply to molecular species with widely different molecular structures and interaction potentials.

3.3. Determination of Surface Tension from Interfacial Region Thickness Values

Equation (73) can be rearranged to the form

$$\sigma_{lv} = 2.36\,(1 - T/T_c)^{0.66}\,\frac{L_i^2}{\delta z_i}\left[T\left(\frac{dP}{dT}\right)_{\text{sat}} - P_{\text{sat}}\right] \tag{74}$$

as described in Appendix D. This relation can be used to compute the interfacial tension if measured values of the other properties on the right side of the equation are available. In some instances, this can provide a useful means of predicting the interfacial tension for conditions under which it is difficult to measure directly. An example is determination of

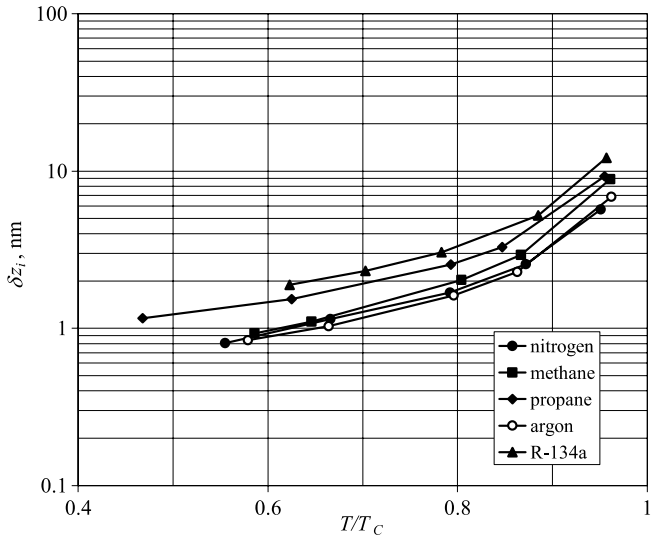

Fig. 2. Variation of interfacial region thickness with reduced temperature predicted using recommended property values from the *ASHRAE Fundamentals Handbook* [13].

the interfacial tension at temperatures approaching the critical point using vapor pressure and interfacial region thickness data.

The methodology described above was used to predict σ_{lv} values for sulfur hexafluoride very close to the critical point. Beysens and Robert [9] used measurements of optical reflectivity to determine values of interfacial region thickness for sulfur hexafluoride at near-critical conditions. These values are listed in Table III. Table IV lists vapor pressure data adapted from Verdelli et al. [14]. Extrapolation of values in Table IV is required to obtain the saturation pressure and its derivative in Eq. (74) for the temperatures associated with the interfacial region thickness data. Figure 3 demonstrates that these values can be approximated by a linear curve fit. Extension of the curve to the temperatures in Table III yields approximate vapor pressure data. The resultant calculated surface tension values from Eq. (74) are shown in Fig. 4 and Table II.

Also shown in this figure is the expected surface tension trend based on an approximated datum. This datum applies vapor pressure data by Verdelli et al. [14] along with critical values recommended by Horvath [18] with relations given by Riedel [16, 17]. The expected trend given by the figure stems from the vanishing of surface tension as the system approaches the critical point and the known power law variation usually observed for pure fluids [8] as the temperature is increased towards the critical point: $\sigma_{lv} \sim (1 - T_r)^{1.22}$. The consistency of this observed trend with this expected

Table III. Calculated Surface Tension Values for Sulfur Hexafluoride Using Eq. (75) and Interfacial Region Thickness Values from Beysens and Robert [9]

$1-T_r$	$P^* \equiv \frac{1}{P_c}\left[T\frac{dP}{dT}-P\right]$	$\frac{\delta z_i}{L_i}$	$\frac{\sigma_{lv}}{L_i P_c}$
0.0010	5.293	71.2	0.0028
0.0013	5.287	66.4	0.0035
0.0015	5.281	56.9	0.0046
0.0019	5.271	47.0	0.0065
0.0025	5.256	37.5	0.0098
0.0030	5.245	37.0	0.0110
0.0035	5.232	28.9	0.0158
0.0040	5.220	27.5	0.0181
0.0044	5.210	33.2	0.0159
0.0048	5.200	29.4	0.0190
0.0055	5.183	28.9	0.0211

Table IV. Vapor Pressure Data from Ref. 14 for Sulfur Hexafluoride Near the Critical Point (extrapolated values italicized)

T (K)	$1-T_r$	P (MPa)	$\frac{dP}{dT}(\text{MPa}\cdot K^{-1})$	$P^* \equiv \frac{1}{P_c}\left[T\frac{dP}{dT}-P\right]$
316.85	0.0058	3.635	0.0730	5.169
312.50	0.0195	3.330	0.0680	4.753
307.50	0.0351	2.995	0.0660	4.589
302.50	0.0508	2.680	0.0600	4.103
297.50	0.0665	2.395	0.0540	3.626
318.48	*0.0010*			*5.293*
318.40	*0.0013*			*5.287*
318.32	*0.0015*			*5.281*
318.19	*0.0019*			*5.271*
318.00	*0.0025*			*5.256*
317.86	*0.0030*			*5.245*
317.68	*0.0035*			*5.232*
317.52	*0.0040*			*5.220*
317.40	*0.0044*			*5.210*
317.27	*0.0048*			*5.200*
317.05	*0.0055*			*5.183*

variation provides some confirmation that the surface tension values computed with this analysis are reliable predictions of this property.

3.4. Surface Tension Determination from Molecular Dynamic Simulation Data

The relations linking interfacial tension to other properties also provide the means to compute the interfacial tension from density gradient

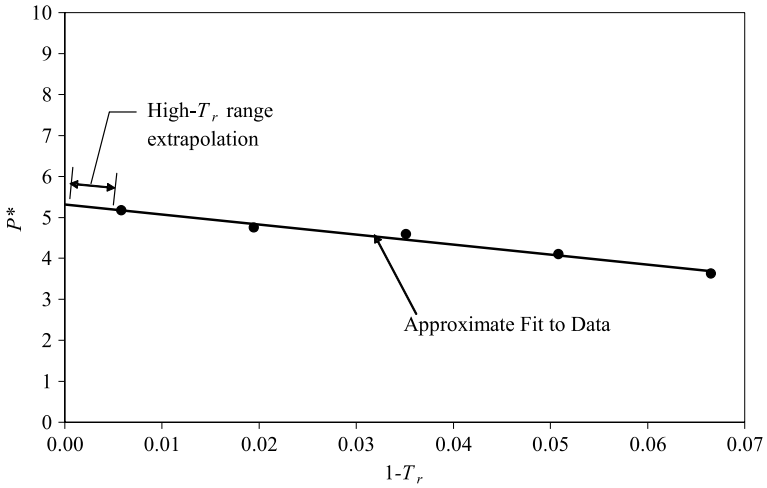

Fig. 3. Extrapolation of a linear fit curve relation to known saturated pressure values to the high-temperature region. Points indicated are recommended values from Verdelli et al. [14].

information obtained from molecular dynamics (MD) simulations. Many MD simulations used to investigate interfacial region thermophysics have used a simulation domain like that shown in Fig. 5. Mean properties are computed in bins within the simulation domain to determine the property variations across the interfacial region. Determination of the mean density variation across the interfacial region is relatively straightforward, and the mean density gradient can be determined from the resulting mean density profile.

The relation for κ given by Eq. (72) is combined with Eq. (44) to generate an explicit relation for interfacial tension,

$$\sigma_{lv} = 0.1065(1 - T/T_c)^{-0.34} L_i^2 \left(\frac{d\hat{\rho}}{dz}\right)_{\hat{\rho}=\hat{\rho}_m} \frac{a_{R0} N_A^2}{b_R N_A T^{1/2}} \ln\left(\frac{1+\hat{\rho}_l b_R N_A}{1+\hat{\rho}_v b_R N_A}\right) \quad (75)$$

To explore this technique for determination of the interfacial tension in MD simulations, MD simulations were constructed for argon using a system of the type shown in Fig. 5. The simulations featured between 2000 and 8000 molecules in a domain in the form of a liquid region sandwiched between two vapor regions. The simulations were initialized with these molecules in a face-centered-cubic close-packed array in the central region. The system was then evolved to an equilibrium configuration by

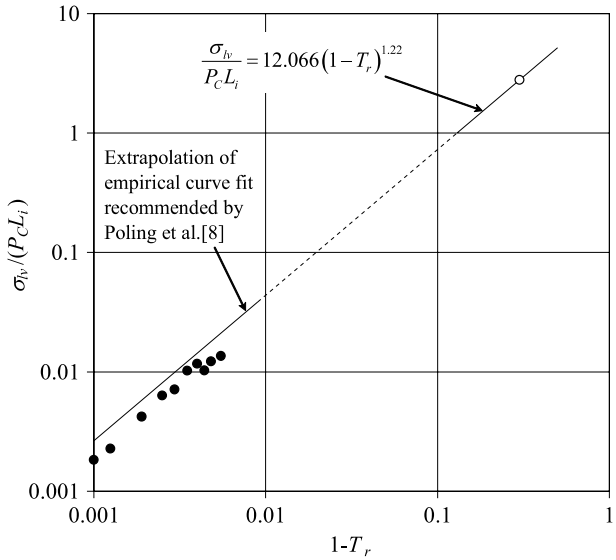

Fig. 4. Comparison of surface tension values found from Eq. (74) (black circles) with the empirically fitted trend to an approximated datum (white circle). Derived values are based on recommended interfacial thickness values from Beysens and Robert [9] and vapor pressure data by Verdelli et al. [14]. Datum is found using methods by Riedel [16, 17] and vapor pressure data by Verdelli et al. [14].

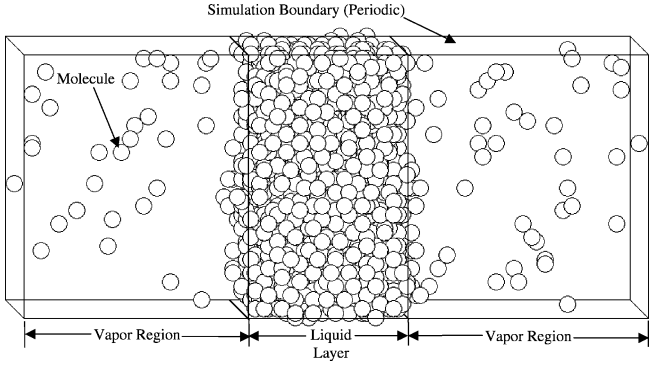

Fig. 5. System snapshot of a typical molecular dynamics simulation, $T_r = 0.65$.

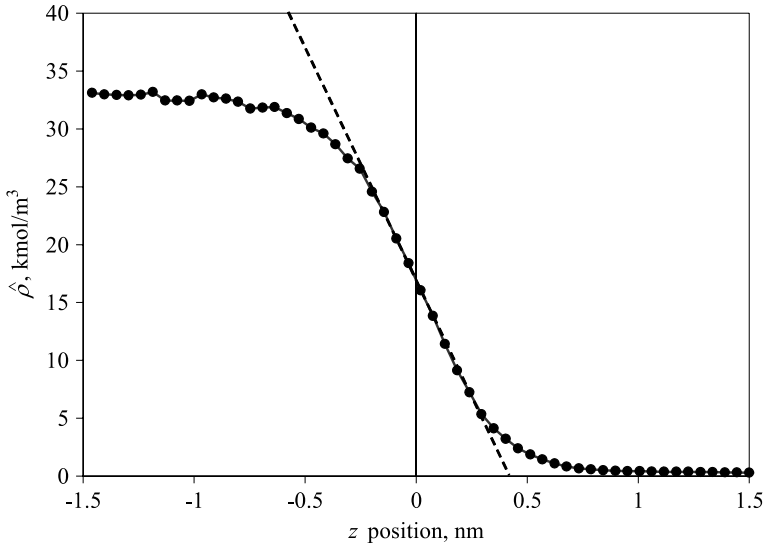

Fig. 6. Argon mean mass density profile through the interfacial region and density gradient at $z = 0$ position (dashed line) by molecular dynamics simulation. Profile shown is for a system of 2064 molecules interacting via the Lennard-Jones potential at $T_r = 0.65$ for 160,000 time steps.

maintaining constant system temperature T and volume V while allowing molecules to interact via the well-known Lennard-Jones 6–12 potential,

$$\phi_{ij}\left(r_{ij}\right) = 4\varepsilon_0\left[\left(\frac{\sigma_{LJ}}{r_{ij}}\right)^{12} - \left(\frac{\sigma_{LJ}}{r_{ij}}\right)^{6}\right], \tag{76}$$

where r_{ij} is the distance between molecules i and j, and σ_{LJ} and ε_0 are the Lennard-Jones length and energy parameters. For our simulations, the values of σ_{LJ} and ε_0 were chosen to be 0.3334 nm and 1.66×10^{-21} J, respectively. The simulations maintained periodic boundary conditions on all faces of the simulation domain. The molecule positions and velocities were updated every time step using the Velocity Verlet algorithm [19], and the time step used was 5 fs. The cutoff distance used in these simulations was $3.0\sigma_{LJ}$ and was applied via the linked-list method as described by Knuth [20] and Hockney and Eastwood [21].

The MD simulations described above were run for reduced temperatures between 0.6 and 0.85. For each simulation, the mean density profile across the interfacial region was determined from the statistical average of density values across the region over time. The density profile obtained for one of the simulations is shown in Fig. 6. For each simulation, the surface

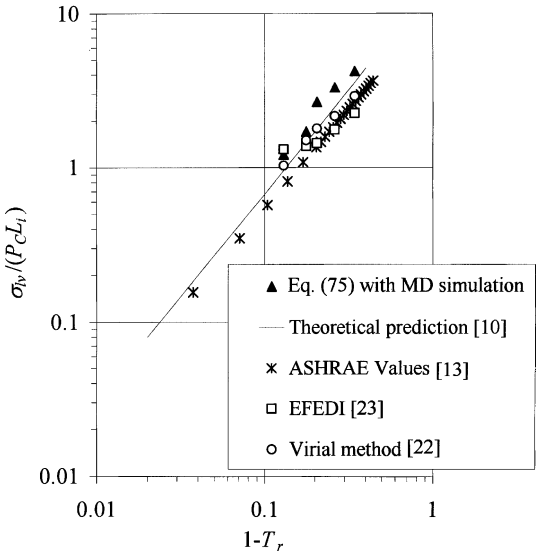

Fig. 7. Surface tension values for argon calculated by Eq. (75) using MD simulations compared to results from other sources.

tension was computed using Eq. (75) with the density gradient determined at the $z=0$ location of the interfacial region as defined by Eq. (1). Calculation of the density gradient was performed by assuming a linear gradient between the two density data points immediately adjacent to the interfacial region position as shown in Fig. 6.

In addition, the surface tension was computed using the virial method [22] that is commonly used to determine the interfacial tension in MD simulations of liquid–vapor interfaces, and through the excess free energy density integration technique (EFEDI) developed by Wemhoff and Carey [23]. The resulting values of surface tension for these three methods are plotted in Fig. 7. Also shown in this figure are the theoretical prediction of Carey's [10] model and recommended data for argon from the *ASHRAE Fundamentals Handbook* [13]. Results using Eq. (76) compare well with trends and magnitudes exhibited by the other models, and they follow the same trend as experimental results. The differences in magnitudes between computational and recommended values determined from experimental data can be attributed to several factors, including adapting an additive potential between molecules in MD simulations, implementing a cutoff distance, and utilizing a finite-sized simulation domain [15]. In addition, Fig. 8 shows that the density gradient values calculated using MD simulations are approximately 25% higher than those predicted by Carey [10].

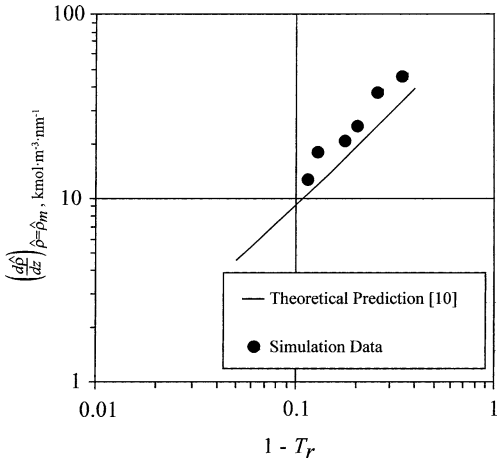

Fig. 8. Predicted interface density gradient values by MD simulation and by Carey [10].

4. CONCLUDING REMARKS

It has been shown that Eqs. (73), (74), and (75) relating surface tension, interfacial region, and density gradient in the interfacial region to other thermodynamic properties can be derived from a model of capillarity that incorporates Redlich-Kwong fluid properties. Models of this type are known to have their limitations, and the relations developed from the model described here are not expected to perfectly match real fluids. However, Carey [10] has shown that this model predicts variations of surface tension and interfacial region thickness that are fairly good matches to real fluid behavior for a variety of fluids including argon, water, propane, and R-134a. These results suggest that the methods presented here may yield useful predictions of the relations among properties. The results of this investigation indicate that Eq. (73) can be useful for generating predictions of interfacial region thickness from other properties. We have also demonstrated that Eq. (74) can be useful as a means of predicting the surface tension from measurements of interfacial region thickness near the critical point.

Perhaps the most useful application of the relations derived here is the use of Eq. (75) for predicting surface tension using density gradient information obtained from MD simulations. It is well known that determination of interfacial tension using the widely used virial method requires inclusion of long-range intermolecular forces [24]. Use of Eq. (75) to predict interfacial tension requires an accurate prediction of the interfacial

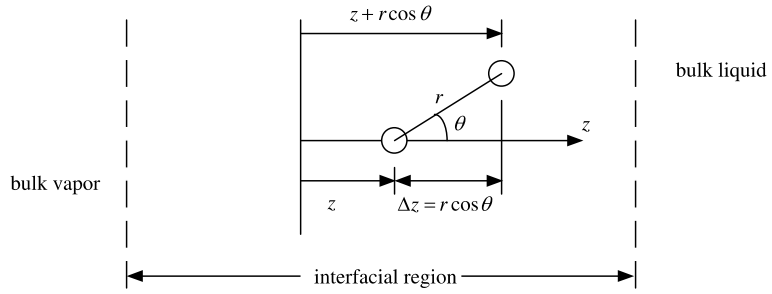

Fig. A1. Pair relative position in interfacial region.

region density gradient. Our results indicate that an accurate prediction of the interfacial region density gradient trend can be obtained using a smaller cutoff distance than is required for determination of the surface tension using the virial method. However, the magnitudes of the gradient values are slightly greater than those predicted by Carey [10], and further study is necessary. This smaller cutoff distance equates to a decreased number of calculations of intermolecular interactions at each time step. In addition, fewer steps are generally required for the density profile to converge to an equilibrium value compared to the number of steps needed to obtain a converged prediction of the surface tension using the virial method [23]. These observations indicate that using Eq. (75) to compute surface tension requires less computational effort than the virial method. Although this type of calculation is somewhat more approximate than the more commonly used virial approach, its computational simplicity may make it a useful alternative that can provide an independent verification of the surface tension values obtained using the virial method.

APPENDIX A. DETERMINATION OF THE PARTITION FUNCTION

Here the intermolecular potential energy interaction is computed using Rayleigh's model (see Fig. A1). For a molecule at an arbitrary z location, the mean energy per molecule is computed by summing the potential energy interaction with all the surrounding molecules and dividing by 2 to assign half the energy to each molecule in the pair. This is represented by the following relation:

$$\frac{\Phi(z)}{N} = \frac{1}{2}\int \rho(z)\phi\, dV, \tag{A1}$$

where ϕ is the radially symmetric molecular interaction potential and Φ is the mean energy per molecule at a location z in the interfacial region. Considering a donut-shaped differential volume dV around the z axis,

$$dV = 2\pi r^2 \sin\theta \, d\theta \, dr$$

we integrate over the entire surrounding space, from an average minimum separation of closest molecules $r_{\min}$ up to a maximum separation distance $r_{\max}$ representing the effective range of the long-range attraction forces between molecules. The resulting volume integral can be cast in the form,

$$\frac{\Phi(z)}{N} = \pi \int_{r_{\min}}^{r_{\max}} \phi(r) r^2 \int_0^{\pi} \rho(r\cos\theta + z) \sin\theta \, d\theta \, dr \tag{A2}$$

As in the van der Waals mean field theory, we expand ρ about a specific z value for small $r\cos\theta$;

$$\rho(r\cos\theta + z) = \rho(z) + \rho'(z) r\cos\theta + \frac{1}{2}\rho''(z) r^2 \cos^2\theta \tag{A3}$$

Substituting the right side of the above equation into Eq. (A2) and integrating with respect to θ yields

$$\frac{\Phi(z)}{N} = 2\pi \int_{r_{\min}}^{r_{\max}} \phi(r) r^2 \, dr + \frac{\pi}{3}\rho''(z) \int_{r_{\min}}^{r_{\max}} \phi(r) r^4 \, dr \tag{A4}$$

As shown by Carey [25], the classic Redlich-Kwong property model amounts to postulating that

$$-2\pi \int_{r_{\min}}^{r_{\max}} \phi(r) r^2 \, dr = a_{R0}\gamma_0(T)\eta_0(V/N) \tag{A5}$$

where γ_0 and η_0 are initially unknown functions of temperature T and inverse density. Note that here V is the volume of a subsystem within the interfacial region in which mean properties are defined. The mean number of molecules in this subsystem is N, and the molecular density is $\rho = N/V$. Consistent with that approach, here we similarly postulate that

$$-\frac{2\pi}{3} \int_{r_{\min}}^{r_{\max}} \phi(r) r^4 \, dr = a_{R1}\gamma_1(T)\eta_1(V/N) \tag{A6}$$

Substituting Eqs. (A5) and (A6) into Eq. (A4) yields

$$\Phi(z) = -a_{R0}\gamma_0(T)\eta_0(V/N)\frac{N^2}{V^2} - \frac{1}{2}a_{R1}\gamma_1(T)\eta_1(V/N)N\rho''(z) \tag{A7}$$

Invoking the idealization that b_R is the mean volume occupied by each molecule in the system and following standard statistical thermodynamic analysis [25], the above relation for Φ can be used to obtain the relation below for the classical configuration integral:

$$Z_N = \exp\left\{\frac{a_{R0}\gamma_0\eta_0 N^2}{Vk_BT} + \frac{a_{R1}\gamma_1\eta_1 N\rho''(z)}{2k_BT}\right\}(V - Nb_R)^N \tag{A8}$$

In Eq. (A8), k_B is the Boltzmann constant. The above relation for Z_N can then be used to obtain the following relation for the natural log of the canonical partition function [25]:

$$\ln Q = N + \left(\frac{3N}{2}\right)\ln\left[\frac{2\pi Mk_BT\,(V - Nb_R)^{2/3}}{N^{2/3}h^2}\right] + N\left[\frac{\xi - 5}{2}\ln\pi - \ln\sigma_s\right] + \frac{(\xi - 3)N}{2}\ln\left(\frac{T}{\theta_{\mathrm{rot},m}}\right) + \frac{a_{R0}\gamma_0\eta_0 N^2}{Vk_BT} + \frac{a_{R1}\gamma_1\eta_1 N\rho''(z)}{2k_BT} \tag{A9}$$

In the above equation, h is Planck's constant, M is the molecular mass of the molecule, ξ is the number of translational and rotational storage modes, σ_s is the symmetry number for the molecule and $\theta_{\mathrm{rot},m}$ is the mean rotational temperature for the molecule if it is a polyatomic species. The equation of state is generated using the following relation for the thermodynamic pressure P from statistical thermodynamics:

$$P = k_BT\left(\frac{\partial \ln Q}{\partial V}\right)_{T,N} \tag{A10}$$

Using Eq. (A9) with $\rho''(z) = 0$ to evaluate the derivative in (A.10) yields the following relation for pressure:

$$P = \frac{Nk_BT}{V - b_RN} - \frac{a_{R0}\gamma_0 N^2}{V}\left(\frac{\eta_0}{V} - \frac{d\eta_0}{dV}\right) \tag{A11}$$

The classical Redlich-Kwong equation of state can be written in the form,

$$P = \frac{Nk_BT}{V - b_RN} - \frac{a_{R0}N^2}{T^{1/2}V(V + b_RN)} \tag{A12}$$

Equivalence of Eqs. (A11) and (A12) requires that

$$\gamma_0 = T^{-1/2} \tag{A13}$$

$$\frac{\eta_0}{V} - \frac{d\eta_0}{dV} = \frac{1}{V + Nb_R} \tag{A14}$$

The differential equation, Eq. (A14), can be solved in closed form to obtain the following solution:

$$\eta_0 = \frac{V}{Nb_R} \ln\left(\frac{V+Nb_R}{V}\right) + C_0 V \tag{A15}$$

where C_0 is an initially unknown constant of integration. For $\rho''(z) = 0$, at fixed T and N, the term in Eq. (A9) containing η_0 must vanish as V becomes large so that the relation for ln Q (Eq. (A9)) approaches the form appropriate for an ideal gas. This can be satisfied using the solution in Eq. (A15) for η_0 only if $C_0 = 0$. It follows that the solutions for γ_0 and η_0 that satisfies this condition and elicit the Redlich-Kwong equation of state from the partition function are

$$\gamma_0 = T^{-1/2} \tag{A16}$$

$$\eta_0 = \frac{V}{Nb_R} \ln\left(\frac{V+Nb_R}{V}\right) \tag{A17}$$

With these definitions, a_{R0} and b_R are the constants in the Redlich-Kwong equation of state for a fluid of uniform density. Equation (A9) can be rearranged to the form,

$$\begin{aligned} \ln Q = N + \left(\frac{3N}{2}\right) \ln\left[\frac{2\pi M k_B T\,(V-Nb_R)^{2/3}}{N^{2/3}h^2}\right] + N\left[\frac{\xi-5}{2}\ln\pi - \ln\sigma_s\right] \\ + \frac{(\xi-3)N}{2}\ln\left(\frac{T}{\theta_{\mathrm{rot,m}}}\right) + \frac{a_{R0}N}{b_R k_B T^{3/2}}\ln\left(\frac{V+Nb_R}{V}\right) \\ + \frac{a_{R0}\kappa V\rho''(z)}{2b_R k_B T^{3/2}}\ln\left(\frac{V+Nb_R}{V}\right) \end{aligned} \tag{A18}$$

where

$$\kappa = \frac{a_{R1}\gamma_1\eta_1}{a_{R0}\gamma_0\eta_0} = \frac{-\frac{2\pi}{3}\int_{r_{\min}}^{r_{\max}} \phi(r) r^4 dr}{-2\pi \int_{r_{\min}}^{r_{\max}} \phi(r) r^2 dr} \tag{A19}$$

APPENDIX B. DETERMINATION OF SATURATION PROPERTIES

To determine the reduced saturation properties for a specified T_r, the following iterative scheme was used:

(i) An initial guess for the reduced saturation pressure $P_{\mathrm{r,sat}}$ was specified.
(ii) Equation (63) was solved explicitly and Eqs. (64a) and (64b) were used to determine $v_{r,v}$ and $v_{r,l}$.

(iii) Reduced saturation densities were computed as $\rho_{r,v} = 1/v_{r,v}$ and $\rho_{r,l} = 1/v_{r,l}$.

(iv) T_r and the computed values of $\rho_{r,v}$ and $\rho_{r,l}$ were substituted into the left side of Eq. (67). If the left side was not sufficiently close to zero, the guessed value of $P_{\mathrm{r,sat}}$ was corrected and steps (ii)–(iv) were repeated. If the absolute value of the left side of Eq. (67) was small ($<10^{-8}$) then the computed values of $\rho_{r,v}$, $\rho_{r,l}$ and $P_{r,sat}$ were taken to be correct and step (v) is executed.

(v) The reduced chemical potential $\mu_{r,v}$ for the saturated vapor was calculated using Eq. (65) with the computed saturation properties $\rho_{r,v}$, $\rho_{r,l}$ and T_r.

The scheme described above computes the bulk equilibrium properties for the liquid and vapor phases based on the Redlich-Kwong model. Carey [10] has shown that this scheme predicts saturation properties that are in fairly good agreement with recommended values from the *ASHRAE Fundamentals Handbook* [13]. Note that once $\rho_{r,v}$, $\rho_{r,l}$ and $\mu_{r,v}$ are determined, the physical properties can be determined from the reduced properties using Eqs. (43a)–(43d) if necessary.

Equation (67), which embodies the requirement that $\hat{\mu}_v = \hat{\mu}_l$ in the above scheme, is obtained by evaluating the μ_r relation of Eq. (65) for vapor and liquid reduced densities and equating the results. It should be noted that Eq. (67) can also be obtained by integrating the differential form of the Gibbs–Duhem equation ($d\hat{\mu} = -\hat{s}\,dT + Pd\hat{v}$) along an isotherm using the equation of state in Eq. (59) to relate P to $\hat{v}$. Saturation property curves obtained using the above scheme are therefore identical to those obtained with the classical "equal areas" method based on integration of the Gibbs–Duhem equation along an isotherm using the Redlich-Kwong equation of state.

APPENDIX C. DETERMINATION OF κ

To complete the model analysis described here, a means of evaluating κ must be provided. This appendix summarizes the model proposed by Carey [10] for determining κ. In the definition of κ specified in Eq. (8), the form of the integral in the numerator is similar to that in the denominator, suggesting that it also is a function of temperature and density. Since consistency with the Redlich-Kwong model seems to require that the numerator and denominators on the right side are functions of temperature and density, in general we expect that κ is a function of temperature and density.

In evaluating κ, we note that the choice of $r_{\min}$ affects the potential energy stored in the system because the potential energy interaction between each pair is dictated by their separation, and $r_{\min}$ is an average

separation of the closest molecules. Contributions of these integrals to the total energy are greatest when the density is highest, so here we pick $r_{\min}$ to be the mean separation of the closest molecules in the bulk saturated liquid phase, where the density is highest. To define the relationship between the saturated liquid number density ρ_l and $r_{\min}$, we model the liquid as a three-dimensional cubic array of molecules with nearest neighbors separated by a center-to-center distance of $r_{\min}$. It follows that

$$\rho_l = \frac{1}{r_{\min}^3} \tag{C1}$$

and therefore

$$r_{\min} = \rho_l^{-1/3} \tag{C2}$$

Since mean field theory is not expected to apply very close to the critical point, we assume that this analysis is at least valid at reduced temperatures less than 0.9 ($T/T_c < 0.9$). Asymptotic analysis of the Redlich-Kwong model predictions of the saturated liquid and vapor densities indicates that for $0.6 < T/T_c < 0.9$

$$\frac{\rho_l - \rho_v}{\rho_c} = 5.15\left(1 - \frac{T}{T_c}\right)^{0.5} \tag{C3}$$

For $T/T_c < 0.9$, $\rho_v \ll \rho_l$, and the above relation implies that

$$\frac{\rho_l}{\rho_c} = 5.15\left(1 - \frac{T}{T_c}\right)^{0.5} \tag{C4}$$

Solving Eq. (C4) for ρ_l and substituting into Eq. (C2) yields

$$r_{\min} = 0.579\rho_c^{-1/3}\left(1 - \frac{T}{T_c}\right)^{-1/6} \tag{C5}$$

For a Redlich-Kwong fluid, it is readily shown that

$$\frac{\rho_c k_B T_c}{P_c} = 3 \tag{C6}$$

Defining

$$L_i = \left[\frac{k_B T_c}{P_c}\right]^{1/3} \tag{C7}$$

and using Eqs. (C6) and (C7), Eq. (C5) can be rearranged to the form,

$$\frac{r_{\min}}{L_i} = 0.4016\,(1 - T/T_c)^{-1/6} \tag{C8}$$

To evaluate κ using Eq. (8), a model potential function $\phi(r)$ is needed. In this investigation, the well-known Lennard-Jones 6–12 potential

model was used

$$\phi = 4\varepsilon_0 \left[\left(\frac{\sigma_{LJ}}{r} \right)^{12} - \left(\frac{\sigma_{LJ}}{r} \right)^{6} \right] \tag{C9}$$

The Lennard-Jones potential was selected because it is generally acknowledged to be among the more realistic two-parameter intermolecular potential function models and because the two-parameter Lennard-Jones potential is consistent with the two-parameter Redlich-Kwong property model used here. Taking $r_{\max} = \infty$ and evaluating the integrals in Eq. (8) using the Lennard-Jones potential function of Eq. (C9), the resulting relation for κ is

$$\kappa = r_{\min}^2 \left[\frac{\left(\frac{r_{\min}}{\sigma_{LJ}} \right)^6 - \frac{1}{7}}{\left(\frac{r_{\min}}{\sigma_{LJ}} \right)^6 - \frac{1}{3}} \right] \tag{C10}$$

It is clear from Eq. (59) that the minimum molar specific volume that the fluid can have for finite pressure is $b_R N_A$ Assuming that this corresponds to cubic close packing of molecules, the volume fraction occupied by the molecules must equal 0.7405. Taking the molecular diameter to be σ_{LJ}, it follows that

$$N_A \left(\frac{4\pi}{3} \right) \left(\frac{\sigma_{LJ}}{2} \right)^3 = 0.7405 b_R N_A \tag{C11}$$

This relation can be rearranged to the form,

$$b_R = 0.7071 \sigma_{LJ}^3 \tag{C12}$$

Combining Eqs. (C6), (60b), and (C12), the following relation is obtained:

$$\sigma_{LJ} = 0.4967 L_i \tag{C13}$$

Using Eq. (C13) to replace σ_{LJ} in Eq. (C10) yields

$$\frac{\kappa}{L_i^2} = \left(\frac{r_{\min}}{L_i} \right)^2 \left[\frac{1 - 0.002146 \, (L_i / r_{\min})^6}{1 - 0.005007 \, (L_i / r_{\min})^6} \right] \tag{C14}$$

Evaluating the ratio $r_{\min}/L_i$ using Eq. (C8) converts this relation to the form,

$$\frac{\kappa}{L_i^2} = 0.1613 \, (1 - T/T_c)^{-0.34} \left[\frac{1 - 0.5117 \, (1 - T/T_c)}{1 - 1.1938 \, (1 - T/T_c)} \right] \tag{C15}$$

Finally, since we are interested in conditions where $1 - T/T_c$ is small, we expand the factor in square brackets for small $1 - T/T_c$ and retain only the first term. This simplifies Eq. (C15) to

$$\frac{\kappa}{L_i^2} = 0.1613\,(1 - T/T_c)^{-0.34} \tag{C16}$$

APPENDIX D. DETERMINATION OF PROPERTY RELATION OF EQ. (74)

Equation (73) can be written as

$$\sigma_{lv} = 0.071 L_i^2\,(1 - T/T_c)^{-0.34} \left(\frac{\hat{\rho}_{lv}}{\delta z_i}\right) \hat{u}_{lv} \tag{D1}$$

where

$$\hat{\rho}_{lv} = \hat{\rho}_l - \hat{\rho}_v \tag{D2}$$

and

$$\hat{v}_{lv} = \hat{v}_l - \hat{v}_v \tag{D3}$$

Asymptotic analysis using the Redlich-Kwong model predicts variations of the molar density and specific volume changes for vaporization as the critical point is approached as

$$\frac{\hat{\rho}_{lv}}{\hat{\rho}_c} = 5.50\left(1 - \frac{T}{T_c}\right)^{0.5} \tag{D4}$$

$$\frac{\hat{v}_{lv}}{\hat{v}_c} = 6.05\left(1 - \frac{T}{T_c}\right)^{0.5} \tag{D5}$$

Substituting Eq. (D4) into Eq. (D1) yields

$$\sigma_{lv} = 0.071(5.50) L_i^2\,(1 - T/T_c)^{0.16}\,\hat{\rho}_c \left(\frac{\hat{u}_{lv}}{\delta z_i}\right) \tag{D6}$$

Combining the Clapeyron equation,

$$\left(\frac{dP}{dT}\right)_{sat} = \frac{\hat{h}_{lv}}{T\hat{v}_{lv}} \tag{D7}$$

with the definition of molar enthalpy,

$$\hat{h}_{lv} = \hat{u}_{lv} + P_{sat}\hat{v}_{lv} \tag{D8}$$

yields the relation for molar internal energy change for vaporization:

$$\hat{u}_{lv} = \hat{v}_{lv}\left[T\left(\frac{dP}{dT}\right)_{\text{sat}} - P_{\text{sat}}\right] \tag{D9}$$

Combination of Eqs. (D5), (D6), and (D9) yields

$$\sigma_{lv} = 2.36\,(1 - T/T_{\text{c}})^{0.66}\,\frac{L_i^2}{\delta z_i}\left[T\left(\frac{dP}{dT}\right)_{\text{sat}} - P_{\text{sat}}\right] \tag{D10}$$

ACKNOWLEDGMENT

Support for this research by Alcoa Aluminum Company is gratefully acknowledged.

NOMENCLATURE

a_{R0}	Redlich-Kwong constant for zero density gradient
b_{R}	Redlich-Kwong constant
$\hat{f}$	molar specific free energy
k_{B}	Boltzmann constant
L_i	interfacial region characteristic length
N_{A}	Avogadro's number
P	pressure
R	universal gas constant
T	temperature
$\hat{v}$	molar specific volume
V	system volume
z	coordinate normal to the interface
δz_i	interfacial region thickness
δz_u	thickness of sublayer lacking intrinsic stability
ε_0	Lennard-Jones energy parameter
ξ	number of translational plus rotational energy storage modes
ρ	number density of molecules
$\hat{\rho}$	molar density
σ	interfacial free energy per unit interfacial area
σ_{lv}	interfacial tension
σ_{LJ}	Lennard-Jones parameter
$\theta_{\text{rot,m}}$	mean rotational temperature
ϕ_{ij}	Lennard-Jones potential
ζ	nondimensional interfacial region position

Subscripts

c critical point property
l saturated bulk liquid
m mean of saturated bulk liquid and vapor properties
v saturated bulk vapor
r reduced property (normalized with critical properties)
sat saturation property

REFERENCES

1. M. Matsumoto, Y. Takaoka, and Y. Kataoka, *J. Chem. Phys.* **98**: 1464 (1993).
2. M. Matsumoto, K. Yasuoka, and Y. Kataoka, *Thermal Sci. Eng.* **2**: 64 (1994).
3. K. Yasuoka, M. Matsumoto, and Y. Kataoka, *Proc. ASME/JSME Thermal Eng. Conf.* **2**: 459 (1995).
4. M. Matsumoto, K. Yasuoka, and Y. Kataoka, *Proc. ASME/JSME Thermal Eng. Conf.* **2**: 465 (1995).
5. L. X. Dang and T. M. Chang, *J. Chem. Phys.* **106**: 8149 (1997).
6. M. Chen, Z. Y. Guo, and X. G. Liang, *Microscale Thermophys. Eng.* **5**: 1 (2001).
7. M. Tarek, D. J. Tobias, and M. L. Klein, *Physica A* **231**: 117 (1996).
8. B. E. Poling, J. M. Prausnitz, and J. P. O'Connell, *The Properties of Gases and Liquids*, 5th Ed. (McGraw Hill, New York, 2000).
9. D. Beysens and M. Robert, *J. Chem. Phys.* **87**: 3056 (1987).
10. V. P. Carey, *J. Chem. Phys.* **118:** 5053 (2003).
11. M. J. Hey and D.W. Wood, *J. Colloid Interf. Sci.* **90**: 277 (1982).
12. I. S. Sokolnikoff and R. M. Redheffer, *Mathematics of Physics and Modern Engineering*, 2nd Ed. (McGraw-Hill, New York, 1966), Chap. 5.
13. *ASHRAE Fundamentals Handbook* (American Society of Heating, Refrigeration and Air-conditioning Engineers, Atlanta, Georgia, 2001).
14. L. S. Verdelli, H. C. Miller, and J. F. Gall, *Ind. Eng. Chem.* **43**: 1126 (1951).
15. J. Weng, S. Park, J. Lukes, and C.-L. Tien, *J. Chem. Phys.* **117**: 5917 (2000).
16. L. Riedel, *Chem. Ing. Tech.* **26**: 83 (1954).
17. L. Riedel, *Chem. Ing. Tech.* **27**: 209 (1955).
18. A. L. Horvath, *Physical Properties of Inorganic Compounds* (Crane Russak, New York, 1975).
19. M. Allen and D. Tildesley, *Computer Simulations of Liquids* (Clarendon, Oxford, London, 1987).
20. D. Knuth, *The Art of Computer Programming*, 2nd Ed. (Addison-Wesley, Reading, Massachusetts, 1973).
21. R. W. Hockney and J. W. Eastwood, *Computer Simulation Using Particles* (McGraw-Hill, New York, 1981).
22. E. Salomons and M. Mareschal, *J. Phys. Cond. Mat.* **3**: 3645 (1991).
23. A. Wemhoff and V. P. Carey, *Proc. 2003 ASME Heat Trans. Conf.*, in press.
24. M. Nijmeijer, A. Bakker, C. Bruin, and J. Sikkenk, *J. Chem. Phys.* **89**: 3789 (1988).
25. V. P. Carey, *Statistical Thermodynamics and Microscale Thermophysics* (Cambridge University Press, Cambridge, United Kingdom, 1999).